Wireless Power Transfer, 2017, 4(1), 42–54. © Cambridge University Press, 2017
doi:10.1017/wpt.2016.14

RESEARCH ARTICLE

Maximizing the efficiency of wireless power transfer with a receiver-side switching voltage regulator

YOSHIAKI NARUSUE[1,2], YOSHIHIRO KAWAHARA[1] AND TOHRU ASAMI[1]

Output voltage regulation is an essential technology for achieving stable wireless power supply. A receiver-side switching voltage regulator is useful for realizing output voltage regulation. However, this paper shows that the switching voltage regulator degrades the transfer efficiency to below 50% in a wireless power transfer system that consists of a class-D power inverter and series-resonant transmitting and receiving resonators. Such efficiency degradation is caused by the instability of an operating point where the efficiency is >50%. The input resistance value of the switching voltage regulator at a stable operating point is much higher than the optimum value for maximizing the efficiency. To stabilize the high-efficiency operating points, this paper formulates a stability condition and derives its sufficient condition. The sufficient condition facilitates a system design method using a K-impedance inverter that allows for the optimum input resistance value to lie in the range of allowable input resistance values. In addition, we introduce an input-voltage-based efficiency maximization method for the system with the receiver-side switching voltage regulator. By combining these two methods, efficiency maximization is realized with the receiver-side switching voltage regulator. The proposed methods were verified by both simulations and measurements.

Keywords: Wireless power transfer, Magnetic resonant coupling, Switching voltage regulator

Received 26 June 2016; Revised 19 November 2016; Accepted 21 November 2016; first published online 8 February 2017

I. INTRODUCTION

Although wireless power transfer (WPT) has been researched for more than a century [1], replacing a power-feeding wire with a wireless connection remains a challenging task. WPT using magnetic resonant coupling was proposed in 2007 [2, 3]. Since then, it has been attracting considerable attention owing to its high efficiency in mid-range power transmission. It is considered to be a key technology for realizing wireless power supply to moving objects such as electric vehicles [4], electric home appliances [5], mobile devices [6], and biomedical devices [7]. To realize these applications, many researchers have been focusing on resonator designs for higher efficiency [8, 9], design methods of highly efficient WPT systems [10], power source designs [11, 12], rectifier designs [13], human exposure [14], and maximum efficiency point tracking using a receiver-side DC–DC converter [15, 16].

It is challenging to realize high-efficiency and stable WPT because of changes in the transmitter and receiver topologies and load. Such changes affect not only the transfer efficiency, but also the output voltage and transferred power. In terms of the stable operation of devices that obtain electric power via WPT, regulation of the output voltage or transferred power is a critical technology for achieving stable power supply. Regulation of the transferred power is often performed by changing the operating frequency and input power [17]. However, this method requires feedback from the receiver side to the transmitter side over wireless communication channels. Thus, transferred power regulation suffers from disconnection and delay of the channel, which result in unstable transferred power. In a system with a receiver-side DC–DC converter for maximum efficiency point tracking, input voltage control allows transferred power adjustment [16]. This method is effective for realizing stable power transfer, but it also depends on the feedback via wireless channels. A sudden change in the receiver's position or load resistance disrupts the transferred power. Gunji *et al.* realized stable output voltage using an active rectifier [18]. By stopping rectification when the output voltage is likely to exceed its desired value, the output voltage can be stabilized. This method does not require wireless communication for output regulation, because such regulation can be realized only on the receiver side. However, the behavior of the active rectifier modulates the currents in resonators. In terms of legal restrictions and electromagnetic compatibility, it is desirable to avoid modulated waveforms.

On the other hand, using a switching voltage regulator is an alternative and convenient approach that can realize stable output voltage without the requirement of feedback from the power receiver to the transmitter, as considered in [19]. Moreover, it does not modulate waveforms. However, the

[1]Graduate School of Information Science and Technology, The University of Tokyo, 7-3-1, Hongo, Bunkyo-ku, Tokyo 113-8656, Japan. Phone: +81-3-5841-6710
[2]JSPS Research Fellow DC1, 5-3-1, Kojimachi, Chiyoda-ku, Tokyo 102-0083, Japan
Corresponding author:
Y. Narusue
Email: narusue@akg.t.u-tokyo.ac.jp

present study shows that a receiver-side switching voltage regulator degrades the transfer efficiency of WPT; the efficiency is <50% in a system with a class-D inverter and series-resonant transmitter and receiver, which is a common configuration. Such efficiency degradation is mainly due to a stable operating point of the switching voltage regulator, as discussed in Section II. The input resistance value of the switching voltage regulator at a stable operating point cannot avoid being much larger than the optimum resistance value for maximizing transfer efficiency, even with the use of conventional efficiency maximization. In other words, operating points where the transfer efficiency is higher than 50% have been found to be unstable.

To overcome the problem mentioned above, the present paper formulates a stability condition and derives its sufficient condition. Accordingly, it is proposed that an output filter be inserted into the class-D inverter. A *K*-impedance inverter inserted as the output filter can extend the range of allowable input resistance values of the switching voltage regulator to include the optimum value. Furthermore, it is shown that efficiency maximization based on the input voltage is effective for a system with a receiver-side switching voltage regulator. However, conventional maximum efficiency point tracking by directly controlling the duty ratio is not applicable because the duty ratio is determined to regulate the output voltage, not to maximize the efficiency. The proposed system design and efficiency maximization method are beneficial to wireless power supply systems of electrical devices that require constant input voltage. Hence, a typical application is supplying power wirelessly to devices that are currently powered by an AC adapter or a USB cable, such as home appliances, mobile phones, and micro-controller boards. We have already presented an overview of the system design with a *K*-impedance inverter and efficiency maximization based on the input voltage, for a WPT system with a switching voltage regulator [20]. However, losses in the rectifier and voltage regulator were not considered in the previous study. The present paper describes a more specific formulation of the stability condition by considering such losses and presents the results of experiments conducted at an operating frequency of 6.78 MHz.

The remainder of this paper is organized as follows. Section II shows that a receiver-side switching voltage regulator prevents high-efficiency WPT owing to its input resistance value at a stable operating point, and the fundamental determination mechanism of the input resistance value is described. Section III formulates the stability condition of operating points on the basis of a lossy equivalent circuit, derives its sufficient condition, and shows that a *K*-impedance inverter can extend the range of allowable input resistance values to include the optimum value. Section IV explains the principle of efficiency maximization based on input voltage adjustment. Section V presents the results of some simulations and experiments. Finally, Section VI concludes the paper.

II. ANALYSIS OF A STABLE OPERATING POINT

In this section, the problem caused by a receiver-side switching voltage regulator is clarified. The problem is related to a stable operating point. Figure 1 shows an analytical model with a receiver-side switching voltage regulator. First, the determination mechanism of its input resistance value R_{sr} is discussed. Here, the operating frequency f_o is 6.78 MHz, and both the transmitting resonator and the receiving resonator have the same resonant frequency, i.e.

$$\omega_o = \frac{1}{\sqrt{L_1 C_1}} = \frac{1}{\sqrt{L_2 C_2}}, \tag{1}$$

where ω_o is the operating angular frequency of $2\pi f_o$. For example, let us consider the input resistance value R_{sr} with the parameters listed in Table 1. Figure 2 shows the output power P_{rcv} from the rectifier and transfer efficiency η_{wpt} as a function of the input resistance value R_{sr} of the switching voltage regulator, where P_{rcv} is defined as $V_{rec}I_{rec}$, P_{in} is the output power from an radiofrequency (RF) power source V_{RF}, P_{load} is the power consumption of the load (calculated as V_{out}^2/R_{load}), and η_{wpt} is defined as P_{load}/P_{in}. In the fundamental analysis described in this section, the rectifier and switching voltage regulator are assumed to be ideal, whereas the analysis described in Section III takes their losses into account. The rectifier was modeled as an ideal full-bridge rectifier. Therefore, it is assumed that

$$R_{rec} = \frac{8}{\pi^2} R_{sr} \tag{2}$$

and that the operation of the rectifier is lossless. The input power P_{sr} ($=V_{rec}I_{sr}$) to the switching voltage regulator is calculated using the power efficiency η_{sr} of the switching voltage

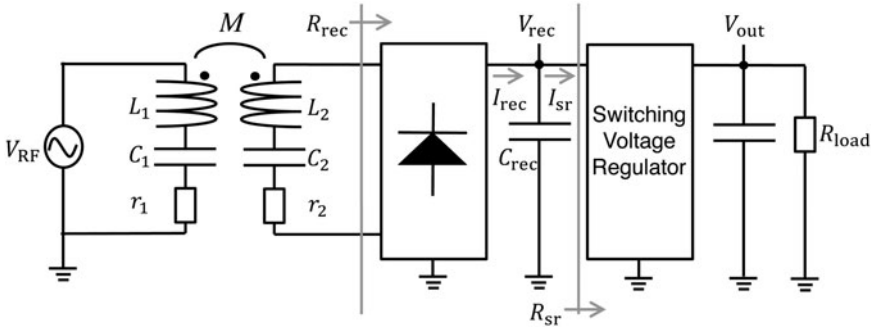

Fig. 1. General block diagram of a wireless power transfer system with a receiver-side switching voltage regulator.

Table 1. Parameters used in the analysis and simulation.

Quantity	Symbol	Value
Operating frequency	f_o (Hz)	6.78×10^6
Operating angular frequency	ω_o (rad/s)	$2\pi \times 6.78 \times 10^6$
Input RF voltage	V_{RF} (V)	6
Inductance of the transmitter	L_1 (μ H)	1
Inductance of the receiver	L_2 (μ H)	1
Mutual inductance between L_1 and L_2	M (H)	$10/\omega_o$
Capacitance of the transmitter	C_1 (pF)	551.037
Capacitance of the receiver	C_2 (pF)	551.037
Resistance of the transmitter	r_1 (Ω)	1
Resistance of the receiver	r_2 (Ω)	1
Output voltage from the regulator	V_{out} (V)	5
Load resistance	R_{load} (Ω)	10

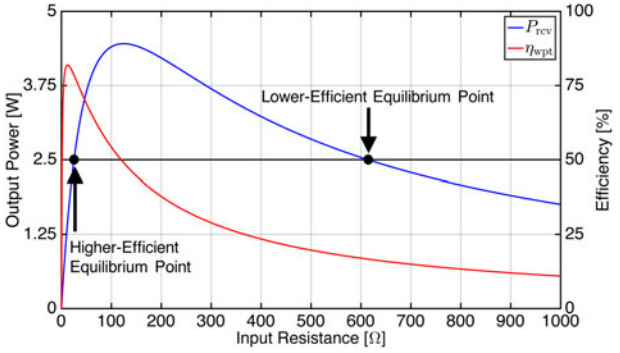

Fig. 2. Output power P_{rcv} from the rectifier and transfer efficiency η_{wpt} as a function of the input resistance value R_{sr} of the switching voltage regulator.

regulator as

$$P_{sr} = \frac{V_{out}^2}{\eta_{sr} R_{load}}. \tag{3}$$

In this section, the loss in the switching voltage regulator is ignored and η_{sr} is assumed to be 1. At a stable operating point, the output power from the rectifier must be equal to the input power to the switching voltage regulator, i.e.,

$$P_{rcv} = P_{sr} \tag{4}$$

must be satisfied. Note that (4) represents an equilibrium condition. Because P_{sr} is $5^2/10 = 2.5$ [W], there are two equilibrium points, and their input resistance value R_{sr} that satisfies (4) is approximately 25.3 or 613.8 Ω according to Fig. 2. The efficiency with R_{sr} of 25.3 Ω is much higher than that with R_{sr} of 613.8 Ω.

The stability of each equilibrium point was investigated. At a stable operating point, even if the output voltage V_{rec} changes from the equilibrium voltage V_{blnc} to $V_{blnc} + \Delta V$, V_{rec} $(= V_{blnc} + \Delta V)$ must return to V_{blnc}. Hence, when V_{rec} increases from the equilibrium voltage V_{blnc} to $V_{blnc} + \Delta V$, $P_{rcv} - P_{sr}$ must be less than zero so that V_{rec} returns to the equilibrium voltage V_{blnc}, i.e.,

$$\frac{d(P_{rcv} - P_{sr})}{dV_{rec}} < 0. \tag{5}$$

If $d(P_{rcv} - P_{sr})/dV_{rec}$ is positive, V_{rec} cannot remain at the equilibrium voltage V_{blnc}. When V_{rec} increases from V_{blnc} to $V_{blnc} + \Delta V$, V_{rec} increases further as $d(P_{rcv} - P_{sr})/dV_{rec} > 0$. In the same way, when V_{rec} decreases from V_{blnc} to $V_{blnc} - \Delta V$, V_{rec} decreases further. This implies that an equilibrium point with $d(P_{rcv} - P_{sr})/dV_{rec} > 0$ is an unstable equilibrium point. Hence, (5) represents the stability condition. Here, we wish to point out that (5) is true even in the case of losses in the rectifier and switching voltage regulator, because the derivation of (5) does not assume lossless operation.

Based on the assumption that the rectifier and switching voltage regulator are ideal, let us judge the stability of each equilibrium point. Equation (5) can be represented using R_{sr} instead of V_{rec} as

$$\frac{d(P_{rcv} - P_{sr})}{dR_{sr}} < 0, \tag{6}$$

because dR_{sr}/dV_{rec} is positive with a constant η_{sr}. Since P_{sr} is 2.5 W regardless of V_{rec}, $dP_{sr}/dR_{sr} = 0$. Further, (6) can be simplified into

$$\frac{dP_{rcv}}{dR_{sr}} < 0. \tag{7}$$

According to Fig. 2, the equilibrium point with R_{sr} of 613.8 Ω satisfies (7), whereas the other equilibrium point with R_{sr} of 25.3 Ω does not. Thus, the actual value of R_{sr} is 613.8 Ω.

To verify the analysis presented above, we conducted a circuit simulation. Figure 3 shows the circuit simulation setup using LTspice. The components used in the simulation were the same as those used in the analysis except for the rectifier and the switching voltage regulator. The rectifier was modeled as a full-bridge rectifier using four Schottky diodes (PMEG4020EPK) and a smoothing capacitor of 10 μ F.

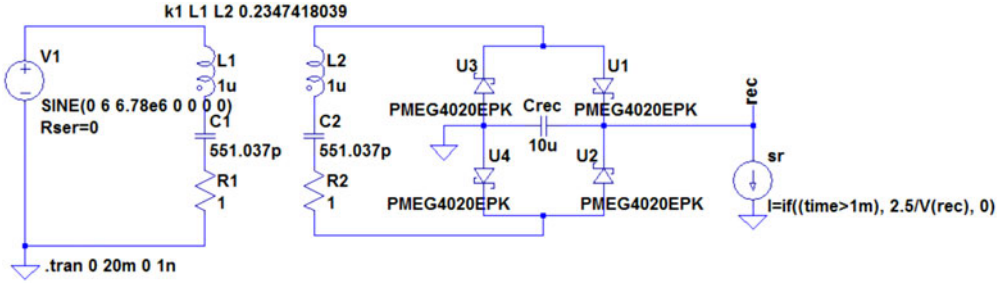

Fig. 3. Simulation setup in LTspice.

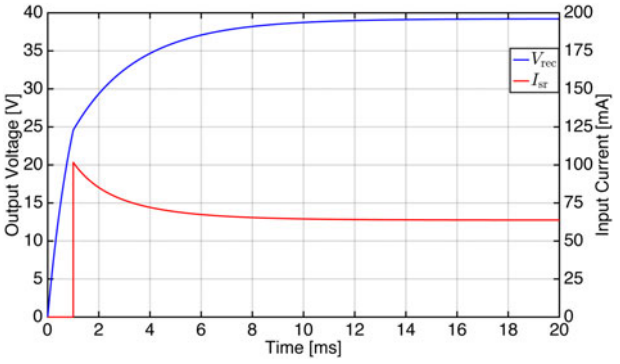

Fig. 4. Simulated output voltage V_{rec} from the rectifier and input current I_{sr} to the switching voltage regulator.

Because the input power to the switching voltage regulator is 2.5 W regardless of V_{rec}, the switching voltage regulator and the load resistance of 10 Ω can be modeled as a component that consumes 2.5 W regardless of V_{rec}. In the simulation on LTspice, the switching voltage regulator and load were modeled as a behavioral current source of $2.5/V_{rec}$ A. Its power consumption was $V_{rec} \times 2.5/V_{rec} = 2.5$ W. Further, the behavioral current source was activated 1 ms after the initiation of the simulation, so that it could store sufficient energy before starting itself up.

Figure 4 shows the simulated V_{rec} and the input current I_{sr} to the switching voltage regulator, which was simulated as the input current to the behavioral current source. The voltage V_{rec} and input current I_{sr} converged to approximately 39.22 V and 63.8 mA, respectively. Hence, the simulated input resistance value R_{sr} at the stable operating point was approximately $39.22/0.638 \sim 615\ \Omega$, which was close to 613.8 Ω. Thus, the simulation result supports the analysis.

The input resistance value R_{sr} of the switching voltage regulator is determined on the basis of (4) and (7). Depending on the input power P_{sr} to the switching voltage regulator, the input resistance values R_{sr} of the equilibrium points also change. However, according to (7) and Fig. 2, the input resistance value R_{sr} cannot be less than the resistance value $R_{sr(mpp)}$ that maximizes the output power P_{rcv} from the rectifier because dP_{rcv}/dR_{sr} is positive when R_{sr} is less than $R_{sr(mpp)}$. Because the output power P_{rcv} is maximized when R_{rec} is equal to

$$R_{rec(mpp)} = \frac{(\omega M)^2}{r_1} + r_2, \tag{8}$$

the resistance value $R_{sr(mpp)}$ is calculated as

$$R_{sr(mpp)} = \frac{\pi^2}{8}\left(\frac{(\omega M)^2}{r_1} + r_2\right) \sim 124.6 \tag{9}$$

using (2). On the other hand, the resistance value $R_{sr(mep)}$ that maximizes the transfer efficiency η_{wpt} is calculated as

$$R_{sr(mep)} = \frac{\pi^2}{8} r_2 \sqrt{1 + \frac{(\omega M)^2}{r_1 r_2}} \sim 12.4 \tag{10}$$

on the basis of (2) and [10]. With the parameters listed in Table 1, $R_{sr(mpp)}$ is much larger than $R_{sr(mep)}$. Hence, WPT at the maximum efficiency point is impossible. In general, $R_{sr(mpp)}$ is larger than $R_{sr(mep)}$ unless $(\omega M)^2$ is equal to o because

$$R_{sr(mpp)}^2 - R_{sr(mep)}^2 = \frac{\pi^4}{64}\left(\frac{(\omega M)^4}{r_1^2} + \frac{r_2(\omega M)^2}{r_1}\right). \tag{11}$$

Thus, the maximum efficiency point, where R_{sr} is $R_{sr(mep)}$, is beyond the stable operating range. Within the stable operating range, the input resistance value of the switching voltage regulator is larger than $R_{sr(mpp)}$, and the transfer efficiency η_{wpt} decreases monotonically as the input resistance value R_{sr} increases according to Fig. 2. Hence, the transfer efficiency η_{wpt} at the stable operating point is less than

$$\eta_{wpt} < \frac{R_{rec(mpp)}}{R_{rec(mpp)} + r_2} \times \frac{(\omega M)^2/R_{rec(mpp)} + r_2}{((\omega M)^2/R_{rec(mpp)} + r_2) + r_1} \tag{12}$$

$$= \frac{((\omega M)^2/r_1) + r_2}{((\omega M)^2/r_1) + 2r_2} \times \frac{((\omega M)^2/((\omega M)^2/r_1) + 2r_2)}{((\omega M)^2/((\omega M)^2/r_1) + 2r_2) + r_1} \tag{13}$$

$$= \frac{(\omega M)^2/r_1 r_2}{2(((\omega M)^2/r_1 r_2) + 2)} \tag{14}$$

$$= \frac{Q_1 Q_2}{2(Q_1 Q_2 + 2)}, \tag{15}$$

where Q_1 and Q_2 are quality factors defined as $\omega M/r_1$ and $\omega M/r_2$, respectively. Even if Q_1 and Q_2 are high, the maximum efficiency at the stable operating point with a switching voltage regulator is <50% according to (15). With the parameters listed in Table 1, the theoretical and simulated values of η_{wpt} are only 16.2 and 17.7%, respectively. On the other hand, the transfer efficiency at the maximum efficiency point without the receiver-side switching voltage regulator is known to be

$$\eta_{wpt} = \frac{Q_1 Q_2}{\left(1 + \sqrt{1 + Q_1 Q_2}\right)^2} \tag{16}$$

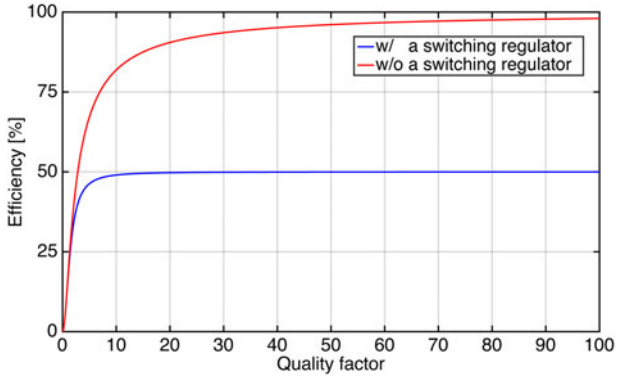

Fig. 5. Comparison between the theoretical efficiencies with and without a receiver-side switching voltage regulator. Each efficiency is plotted as a function of a quality factor $Q = Q_1 = Q_2$.

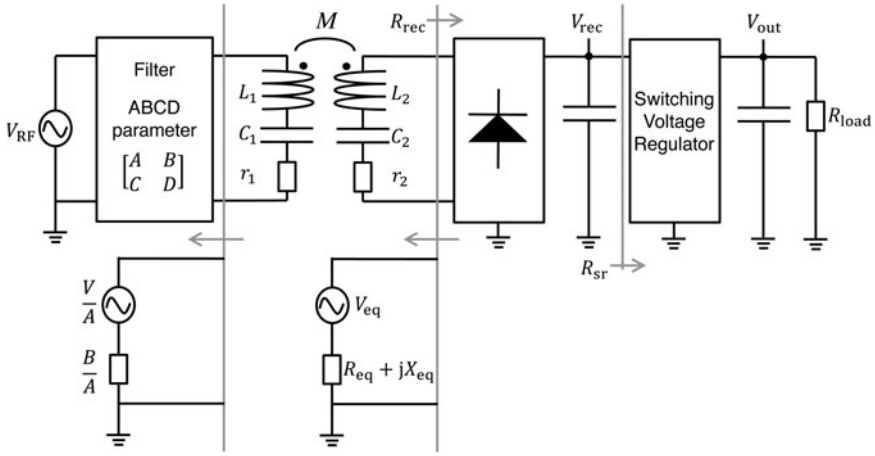

Fig. 6. System configuration with an output filter connected to the output of a power source.

according to [10]. The theoretical maximum efficiency with the parameters listed in Table 1 is 81.9%. Figure 5 shows the theoretical maximum efficiencies with and without a receiver-side switching voltage regulator as a function of a quality factor $Q = Q_1 = Q_2$. As the quality factor increases, the theoretical maximum efficiency without a switching regulator approaches 100%. However, the maximum efficiency with a switching regulator cannot exceed 50%.

To realize high-efficiency WPT, the input resistance value $R_{sr(mep)}$ should be in the stable operating range. If $R_{sr(mpp)}$ is less than $R_{sr(mep)}$, then $R_{sr(mep)}$ is in the stable operating range. The next section describes a system design using a K-impedance inverter to decrease $R_{sr(mpp)}$.

III. STABILIZATION OF THE MAXIMUM EFFICIENCY POINT

This section discusses the stability condition that takes into account the losses in the rectifier and switching voltage regulator. In addition, it describes a system design using a K-impedance inverter to realize stable operation at the maximum efficiency point. Figure 6 shows an analytical model with an output filter inserted between the RF power source and the transmitting resonator. By inserting an appropriate output filter, we aim to stabilize the input resistance value of $R_{sr(mep)}$, which does not change if there is a slight loss in the output filter.

The stability of the input resistance value R_{sr} is determined by (5) even in the case of losses in the rectifier and switching voltage regulator, because the derivation of (5) is not based on the lossless conditions of the rectifier and regulator. However, it is difficult to design the output filter directly from (5). For designing a suitable output filter, it is necessary to represent (5) by using the $ABCD$-matrix of the output filter and variables in the equivalent circuit shown in Fig. 6.

In the analysis, the rectifier was assumed to be a full-bridge rectifier with four Schottky barrier diodes. It is known that a full-bridge rectifier can be precisely analyzed by modeling each Schottky barrier diode as an ideal switch with a voltage drop V_t equal to the barrier height of the diode and a series resistance R_s, as shown in Fig. 7 [21]. Assuming a sinusoidal current input of I to the full-bridge rectifier, the input voltage V_{rec_in} to the rectifier is represented as

$$V_{rec\_in} = \frac{4}{\pi}(V_{rec} + 2V_t)\frac{I}{|I|} + 2R_sI. \tag{17}$$

By applying Kirchhoff's voltage law (KVL), we get

$$V_{eq} = I(R_{eq} + jX_{eq}) + \frac{4}{\pi}(V_{rec} + 2V_t)\frac{I}{|I|} + 2R_sI, \tag{18}$$

where V_{eq} and $R_{eq} + jX_{eq}$ are the equivalent voltage and impedance of Thévenin's equivalent circuit, respectively. Calculating the square of the absolute value of each side gives

$$\left(R_{sum}^2 + X_{eq}^2\right)|I|^2 + 2V_{sum}R_{sum}|I| + \left(V_{sum}^2 - |V_{eq}|^2\right) = 0, \tag{19}$$

where V_{sum} and R_{sum} are defined as $4(V_{rec} + 2V_t)/\pi$ and $R_{eq} + 2R_s$, respectively. Hence, $|I|$ can be solved as

$$|I| = \frac{-V_{sum}R_{sum} + \sqrt{|V_{eq}|^2R_{sum}^2 - \left(V_{sum}^2 - |V_{eq}|^2\right)X_{eq}^2}}{R_{sum}^2 + X_{eq}^2}. \tag{20}$$

The output current I_{rec} from the rectifier is calculated as $2|I|/\pi$, and it is a DC current. Because the output power from the rectifier is calculated as

$$P_{rcv} = \frac{2}{\pi}|I|V_{rec}, \tag{21}$$

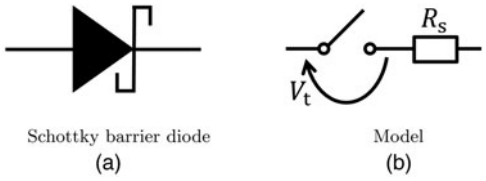

Fig. 7. Modeling of a Schottky barrier diode using an ideal switch with the voltage drop V_t equal to its barrier height and a series resistance R_s.

dP_{rcv}/dV_{rec} is calculated as follows:

$$\frac{dP_{rcv}}{dV_{rec}} = \frac{2}{\pi}|I| - \frac{8}{\pi^2}V_{rec}\frac{R_{sum} + V_{sum}X_{eq}^2/\alpha}{R_{sum}^2 + X_{eq}^2}, \tag{22}$$

where α is given by $\sqrt{|V_{eq}|^2 R_{sum}^2 - \left(V_{sum}^2 - |V_{eq}|^2\right)X_{eq}^2}$. Hence, (5) is represented as

$$\frac{2}{\pi}|I| - \frac{8}{\pi^2}V_{rec}\frac{R_{sum} + V_{sum}X_{eq}^2/\alpha}{R_{sum}^2 + X_{eq}^2} - \frac{dP_{sr}}{dV_{rec}} < 0. \tag{23}$$

Here, we consider the stability condition of the equilibrium point where (4) is satisfied. From (4), (20), and (21),

$$|I| = \frac{-V_{sum}R_{sum} + \alpha}{R_{sum}^2 + X_{eq}^2} = \frac{\pi P_{sr}}{2V_{rec}} \tag{24}$$

holds. Further, (23) is transformed into

$$\frac{P_{sr}}{V_{rec}} - \frac{8}{\pi^2}V_{rec}\frac{R_{sum} + \left(V_{sum}X_{eq}^2/V_{sum}R_{sum} + \left(R_{sum}^2 + X_{eq}^2\right)(\pi P_{sr}/2V_{rec})\right)}{R_{sum}^2 + X_{eq}^2} < \frac{dP_{sr}}{dV_{rec}}. \tag{25}$$

Finally, (25) is simplified into

$$-\frac{8}{\pi^2}\left(\frac{1 + \beta R_{sum}}{R_{sum} + \beta\left(R_{sum}^2 + X_{eq}^2\right)}\right) < \frac{dI_{sr}}{dV_{rec}}, \tag{26}$$

where β is defined as $\pi P_{sr}/(2V_{sum}V_{rec})$. In the last transformation,

$$\frac{dI_{sr}}{dV_{rec}} = \frac{d}{dV_{rec}}\left(\frac{P_{sr}}{V_{rec}}\right) = \frac{1}{V_{rec}}\frac{dP_{sr}}{dV_{rec}} - \frac{P_{sr}}{V_{rec}^2} \tag{27}$$

was applied. By measuring all the variables in (26) around the maximum efficiency point, it is possible to judge whether the maximum efficiency point is stable. However, a system design using (26) is not straightforward.

To realize an easier system design, we propose the use of the sufficient condition of (26) instead of (26) itself. By ignoring

$$\frac{\left(V_{sum}X_{eq}^2\right)}{\left(V_{sum}R_{sum} + \left(R_{sum}^2 + X_{eq}^2\right)(\pi P_{sr}/2V_{rec})\right)} \geq 0$$

in (25),

$$-\frac{8}{\pi^2}\left(\frac{R_{sum}}{R_{sum}^2 + X_{eq}^2}\right) < \frac{dI_{sr}}{dV_{rec}} \tag{28}$$

is derived as a sufficient condition. Using this inequality is beneficial because the switching voltage regulator can be independently evaluated. The right-hand side does not include the variables of the filter, resonators, or rectifier. Moreover, the left-hand side does not include the variables of the switching voltage regulator. The left-hand side of (28) decreases as $|X_{eq}|$ and R_{sum} approaches 0 and $|X_{eq}|$, respectively. Because R_{sum} is positive owing to R_s, the left-hand side of (28) is minimized when $|X_{eq}|$ is 0 and R_{sum} is minimized. The output filter should be designed to realize sufficiently small values of R_{sum} and $|X_{eq}|$ in order to satisfy (28) in the operating range including the maximum efficiency point. We wish to point out that (28) is equivalent to (26) when $|X_{eq}|$ is 0, because

$$\frac{\left(V_{sum}X_{eq}^2\right)}{\left(V_{sum}R_{sum} + \left(R_{sum}^2 + X_{eq}^2\right)(\pi P_{sr}/2V_{rec})\right)}$$

is also 0 when $|X_{eq}|$ is 0. Hence, the sufficient condition (28) approaches the original inequality (26) as $|X_{eq}|$ decreases.

In this paper, we propose the use of a K-impedance inverter as an effective filter. Because R_{sum} and X_{eq} are calculated as

$$R_{sum} = Re\left(\frac{(\omega M)^2}{(B/A) + r_1}\right) + r_2 + 2R_s, \tag{29}$$

$$X_{eq} = Im\left(\frac{(\omega M)^2}{(B/A) + r_1}\right) \tag{30}$$

by using the $ABCD$-matrix of the output filter and the parasitic resistance values in the resonators shown in Fig. 6, an output filter with sufficiently large $|B/A|$ is necessary.

As an output filter with an extremely large $|B/A|$, a K-impedance inverter is one solution. A K-impedance inverter can be realized by a T-network, a Π-network, or coupled

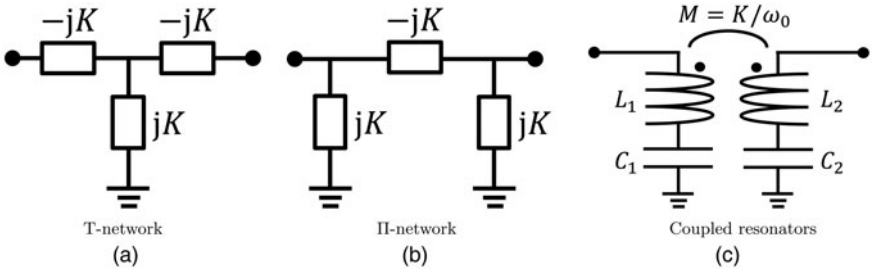

Fig. 8. Examples of circuit configurations of a K-impedance inverter. (a) T-network, (b) Π-network, (c) Coupled resonators whose resonant frequencies are equal to the operating frequency f_0 ($f_0 = 1/(2\pi\sqrt{L_1C_1}) = 1/(2\pi\sqrt{L_2C_2})$).

resonators, as shown in Fig. 8. Its function is to convert the impedance of Z into K^2/Z. It has been used to analyze or design the coupling between resonators in WPT [10, 22, 23]. The $ABCD$-matrix of a K-impedance inverter is represented as

$$F = \begin{bmatrix} 0 & -jK \\ \frac{1}{jK} & 0 \end{bmatrix}. \tag{31}$$

Hence, $|B/A|$ is infinity. When $|B/A|$ is infinity, $R_{sum} = r_2 + 2R_s$ and $X_{eq} = 0$. Then, (28) can be converted into

$$-\frac{8}{\pi^2(r_2 + 2R_s)} < \frac{dI_{sr}}{dV_{rec}}. \tag{32}$$

Note that (32) represents the limitation of the proposed method. The proposed method is not effective for combinations of devices that do not satisfy (32).

Besides the K-impedance inverter, there are other filters with large $|B/A|$. However, the advantaged of the K-impedance inverter is that it does not affect the power factor. When the impedance seen from the input of the transmitter is purely resistive, the input impedance of the K-impedance inverter is also purely resistive. On the other hand, there is an alternative way to design an output filter that consists only of reactance elements to minimize the loss in the filter. Because A of the $ABCD$-matrix should be 0 to realize large $|B/A|$, the $ABCD$-matrix of the filter with only reactance elements can be represented as

$$F = \begin{bmatrix} 0 & -jx_1 \\ \frac{1}{jx_1} & x_2 \end{bmatrix}, \tag{33}$$

where x_1 and x_2 are real numbers. For example, the output filter with the $ABCD$-matrix of (33) can be realized using a K-impedance inverter with $K = x_1$ and a lumped reactance element with an impedance of $j\,x_1x_2$, as shown in Fig. 9.

To verify the effectiveness of the K-impedance inverter, we conducted a circuit simulation. The components were the same as those presented in Section II except for the insertion of a K-impedance inverter with $K = 10$. The K-impedance inverter was modeled using a T-network circuit including two series inductors of 234.7 nH and a shunt capacitor of 2.347 nF. The simulated V_{rec}, I_{sr}, and η_{wpt} were 2.586 V, 967 mA, and 52.2%, respectively. The R_{sr} value of the operating point was just 2.586/0.967~2.67 Ω, which was smaller than $R_{sr(mep)}$. Thus, the maximum efficiency point was in a stable operation range. However, to maximize the transfer efficiency, R_{sr} should be adjusted to $R_{sr(mep)}$. The next section describes an efficiency maximization method based on input voltage control.

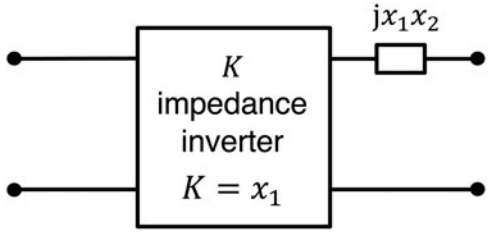

Fig. 9. Realization of (33) with a K-impedance inverter of $K = x_1$ and a lumped reactance element with its impedance of $j\,x_1x_2$.

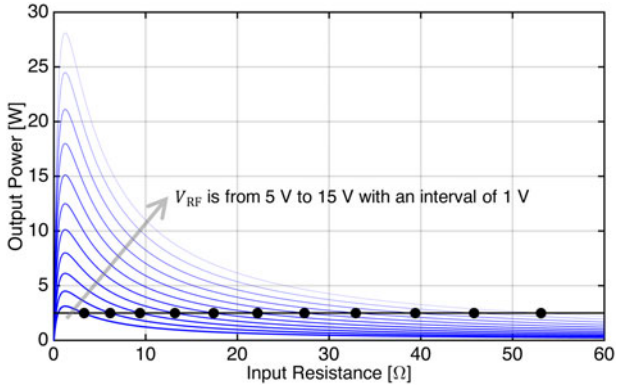

Fig. 10. Output power P_{rcv} as a function of the input resistance value R_{sr} in a system with a K-impedance inverter of $K = 10$ when the input voltage value V_{RF} is from 5 to 15 V.

IV. MAXIMIZING EFFICIENCY BY INPUT VOLTAGE ADJUSTMENT

Recently, a maximum efficiency point tracking method using a receiver-side DC–DC converter has been studied extensively. A switching voltage regulator is a type of DC–DC converter, but it is impossible to control its duty ratio to maximize efficiency because the duty ratio is controlled to regulate the output voltage. However, the duty ratio depends on the ratio of V_{out} and V_{rec}. Moreover, V_{rec} depends on the input voltage V_{RF}. Here, maximum efficiency point tracking is realized by controlling the duty ratio indirectly via input voltage control. Figure 10 shows the theoretical output power P_{rcv} from the rectifier when the input voltage V_{RF} varies from 5 to 15 V. As the input voltage V_{RF} increases, the input resistance value of the stable operating point denoted by a black circle also increases. Figure 11 shows the simulated R_{sr} and transfer efficiency η_{wpt} with a K-impedance inverter of a T-network circuit including two inductors of 234.7 nH and a capacitor of 2.347 nF. As the input voltage value V_{RF} increases, the input resistance R_{sr} also increases in the simulation. Depending on the change in R_{sr}, the transfer efficiency η_{wpt} has one peak. When the input voltage V_{RF} is around

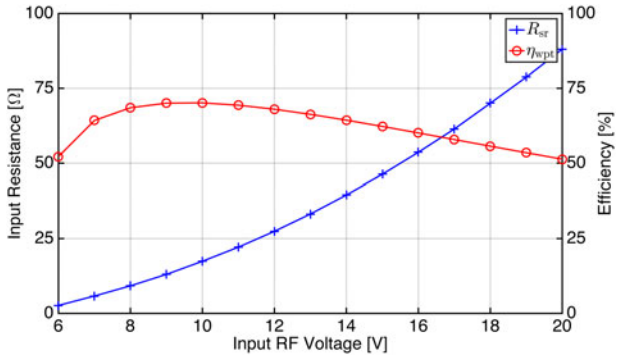

Fig. 11. Simulated transfer efficiency η_{wpt} and output voltage V_{rec} as a function of the input voltage value with a K-impedance inverter of $K = 10$.

10 V, the transfer efficiency is maximized (70.1%) and R_{sr} is 17.4 Ω. These results validate the proposed efficiency maximization based on input voltage control with the switching voltage regulator. By monitoring the output power from the RF power source (P_{in}) while changing its voltage value V_{RF}, the input voltage value $V_{RF(opt)}$ that minimizes the output power P_{in} can be obtained. Further, $V_{RF(opt)}$ is the optimum input voltage value of the RF power source V_{RF} because the power consumption of the load is V_{out}^2/R_{load}, which is a constant. The simulated optimum R_{sr} of 17.4 Ω is larger than the theoretical $R_{sr(mep)}$, which is 12.4 Ω. The difference is attributed to the losses in the rectifier. In general, the power conversion efficiency of the rectifier increases with V_{rec}. Thus, higher R_{sr} enhances the efficiency of the rectifier. The proposed efficiency maximization is effective in enhancing the efficiency of both the coupled resonators and the rectifier. We note that the maximum efficiency realized by the proposed method is slightly lower than that realized by conventional DC–DC converter-based methods because the *K*-impedance inverter has a small loss. However, as described in Section V, the efficiency of the *K*-impedance inverter is virtually negligible. In the experiments described in Section V, the efficiency is more than 97.5%.

V. MEASUREMENTS AND SIMULATIONS

To confirm the validity of the proposed methods, we implemented a WPT system with a *K*-impedance inverter and conducted experiments at an operating frequency of 6.78 MHz. In addition, circuit simulations using LTspice were conducted with the measured parameters of the fabricated devices, and the results were compared with measurement results.

In the measurements and simulations, the output voltage of the switching voltage regulator was 5 V and the load resistance was 10 Ω, assuming power supply to USB 1.x and 2.0 devices in a desktop environment. The voltage rating of USB 1.x and 2.0 devices is 5 V, while their power limitation is 2.5 W. Further, 10 Ω is the load resistance required to consume 2.5 W. As the switching voltage regulator and load of 10 Ω, V7805-1000 (CUI Inc.) and LN-300A-G7 (KEISOKU GIKEN) were used, respectively. In this study, the off-the-shelf switching voltage regulator V7805-1000 was utilized. We believe that an off-the-shelf switching voltage regulator is useful because it facilitates the design and fabrication of power-receiving devices. According to the data sheet of V7805-1000, its input voltage ranges from 6.5 to 32 V, the maximum output current is 1 A, and the power conversion efficiency ranges from 88 to 93%. An *n*-channel MOSFET (PSMN050-80PS) was inserted as shown in Fig. 12 to activate V7805-1000 after storing sufficient energy in C_{rec} to activate it. The drain–gate voltage v_{ds} was controlled using Arduino MEGA. Further, the V–I characteristics of the switching voltage regulator were measured using a power analyzer (Hioki E.E. Corp. PW6001) and a DC power supply (TDK-Lambda Z60-7) in a constant voltage mode, as shown in Fig. 13. Based on the measured values, the range of the input resistance value was calculated as around 12–100 Ω. In addition, dI_{sr}/dV_{rec}, which is the right-hand side of (28), was calculated numerically, as shown in Fig. 13; its minimum value is approximately −0.0565. Hence, if the left-hand side of (28) is less than −0.0565, any input voltage from 6.5 to 32 V is in the stable operating range.

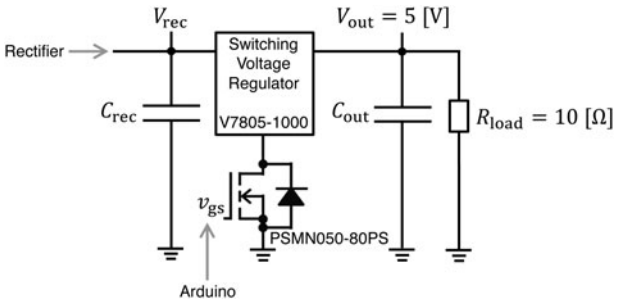

Fig. 12. Connection between V7805–1000 and the load of 10 Ω. An MOSFET is inserted for enabling or disabling the switching voltage regulator.

Figure 14 shows the fabricated transmitting resonator and receiving resonator. Both consist of copper wire having a diameter of 1 mm. As the capacitors, polypropylene film capacitors of the KEMET R73 or R74 series were used. The transmitting resonator was a helical coil around a polystyrene foam core, having 4 turns, a diameter of 30 cm, and a pitch of 1 cm; it was connected in series with a capacitor of 62.2 pF. Further, its input impedance was $1.92 - j0.34$ Ω. The receiving resonator was a spiral coil around an acrylic plate, having five turns and an inner diameter of 10 cm; it was connected in series with a capacitor of 100 pF. Further, its input impedance was $1.78 + j0.67$ Ω. The parameters of the resonators are listed in Tables 2 and 3. In the measurements, the vertical displacement of the receiving resonator was 0, 2, 4, and 6 cm from the

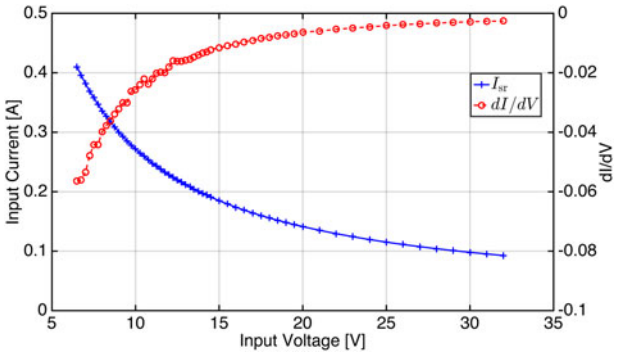

Fig. 13. Measured input current to V7805–1000 and the right-hand side of (29) as a function of the input voltage value.

Fig. 14. Fabricated resonators: (a) transmitter and (b) receiver.

Table 2. Parameters of the fabricated transmitting resonator.

Quantity	Value
Type	Helical
Number of turns	4
Pitch (cm)	1
Inductance (μ H)	11.5
Capacitance attached (pF)	51.9
Resistance (Ω)	1.92
Input impedance (Ω)	$1.92 - j0.34$

Table 3. Parameters of the fabricated receiving resonator.

Quantity	Value
Type	Spiral
Number of turns	5
Inductance (μ H)	5.47
Capacitance attached (pF)	100
Resistance (Ω)	1.78
Input impedance (Ω)	$1.78 + j0.67$

top of the transmitting resonator. By using the measured mutual inductances and the parasitic resistance of each resonator, we calculated the optimum input resistance value R_{rec} of the rectifier on the basis of [10]. The measured mutual inductance, optimum input resistance value R_{rec}, and theoretical maximum efficiency with each vertical displacement are listed in Table 4. From the optimum value of R_{rec}, the optimum input resistance value R_{sr} of the switching regulator was calculated as 23.2, 20.8, 17.9, and 15.1 Ω by using (2). All these values are in the range of the input resistance value of V7805-1000.

To stabilize the maximum efficiency point, a K-impedance inverter was fabricated. In this measurement, the K-impedance inverter was fabricated using coupled resonators as shown in Fig. 8(c). The optimum resistance value for minimizing the loss in the K-impedance inverter using coupled resonators can be calculated in the same way as that for WPT because their configurations are the same. Figure 15(a) shows the K-impedance inverter fabricated using a ferrite core (EPCOS B62152A1X1). Fig. 15(b) shows the equivalent circuit and measured parameters. Because the input impedance Z_{in} seen from the input of the transmitting resonator when R_{rec} is optimum can be calculated as

$$Z_{in} = r_1 + \frac{(\omega M)^2}{r_2 + R_{rec(mep)}} = r_1 + \frac{(\omega M)^2}{r_2 + r_2\sqrt{1 + ((\omega M)^2/r_1 r_2)}}, \quad (34)$$

the theoretical values of Z_{in} with vertical displacements of 0, 2, 4, and 6 cm are 30.8, 27.7, 23.9, and 20.1 Ω, respectively. It is important to design a highly efficient K-impedance inverter with an input impedance of 20.1–30.8 Ω. Their average value is approximately 25.6 Ω. We adjusted the number of turns of each inductor such that the input resistance value for minimizing the loss in the K-impedance inverter would be close to 25.6 Ω. As a result, the number of turns of the inductor connected to port 1 was one and the number of turns of the other inductor was two. When the RF power source was connected to port 1 of the K-impedance inverter, the optimum impedance connected to port 2 was calculated as 34.2 Ω. On the other hand, when port 2 was connected to the power source, the optimum impedance of port 1 was 22.4 Ω. Hence, port 2 was connected to the RF power source and port 1 was connected to the transmitter. Figure 16 shows the efficiency of the fabricated K-impedance inverter when a resistive load is connected to its port 1. The efficiency was calculated using the measured parameters of the fabricated K-impedance inverter and defined as the power consumption of the resistance connected to port 1 divided by the input power from port 2. From 15 to 33.5 Ω, the efficiency was >97.5%. Hence, the loss in the K-impedance inverter has an insignificant effect on the overall efficiency of the implemented wireless power system. When the range of input impedances is too wide to be covered by a single K-impedance inverter, connecting several K-impedance inverters via switches and activating only one of them is an effective approach. It is noted that a K-impedance inverter should be fabricated with heat sinks when the transferred

Table 4. Mutual inductances, optimum resistances, and theoretical maximum efficiencies.

Displacement (cm)	Mutual inductance (nH)	Optimum load (Ω)	Maximum efficiency (%)
0	695	28.6	88.3
2	624	25.7	87.0
4	537	22.1	85.1
6	451	18.6	82.5

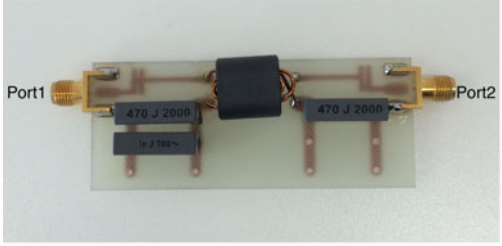

Fabricated K-impedance inverter
(a)

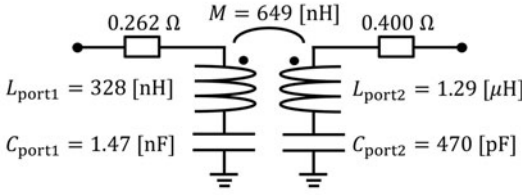

Equivalent circuit
(b)

Fig. 15. Fabricated K-impedance inverter and its equivalent circuit.

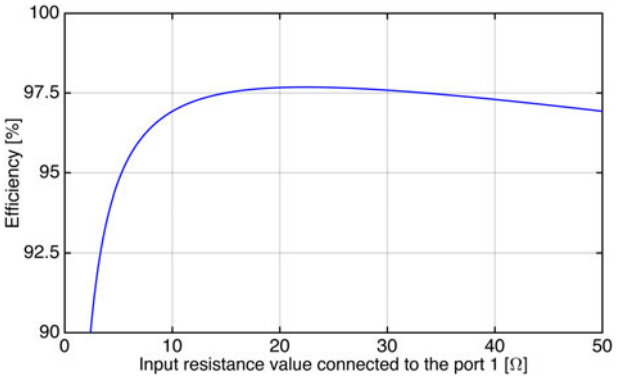

Fig. 16. Efficiency of the fabricated *K*-impedance inverter as a function of the input resistance value connected to its port 1.

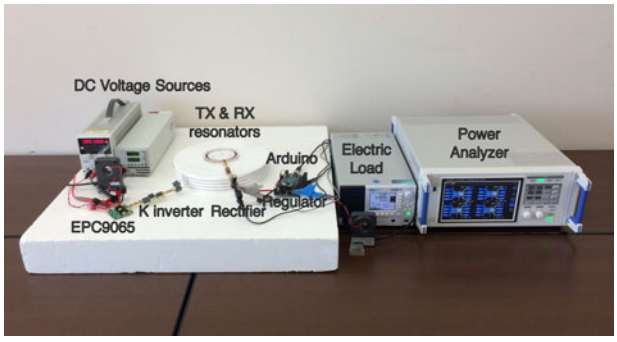

Fig. 17. Experimental setup.

power is sufficiently high to cause heating of the *K*-impedance inverter.

As the RF power source, a class-D zero voltage switching full-bridge inverter (EPC9065) was used. We used a DC voltage sources (TDK-Lambda Z60-7 and TEXIO PA18-3B) in a constant voltage mode as the main power source and logic supply to EPC9065. A full-bridge rectifier was implemented using PMEG4020EPK diodes, a ceramic capacitor of 10 μ F, and an aluminum electrolytic capacitor of 470 μ F. We measured the equivalent impedance $R_{eq} + jX_{eq}$ by using a vector network analyzer (Rohde & Schwarz ZVL3). During the measurements, port 1 of the *K*-impedance inverter was connected to the transmitting resonator and port 2 was a short circuit because the output impedance of a class-D inverter can be approximated as 0 Ω [24, 25]. Table 5 lists the measured values of $R_{eq} + jX_{eq}$. According to the data sheet of PMEG4020EPK, V_t and R_s were approximated as 0.395 V and 95 m Ω. Therefore, the left-hand side of (28) can be calculated as −0.307, −0.339, −0.371, and −0.400 with vertical displacements of 0, 2, 4, and 6 cm, respectively. The maximum value of the left-hand side of (28) was −0.307; hence, the value of the left-hand side was always less than the minimum value of the right-hand side of (28) at any vertical displacement. Thus, the overall input voltage of the switching voltage regulator is in the stable operating range, as is the maximum efficiency point.

Figure 17 shows the measurement setup, and the block diagram of the measurement setup is shown in Fig. 18. Figure 19 shows the simulation setup. In the simulations, an RF power source was modeled using two square-wave voltage sources having a duty ratio of 50%. The switching regulator was also modeled as a behavioral current source of 2.5/0.9 W, assuming that the power conversion efficiency of the switching voltage regulator was 90%. Figure 20(a) shows the measured efficiency η_{meas}. The measured efficiency η_{meas} was defined as the power consumption P_{out} of the load of 10 Ω divided by the input power P_{in} from a constant DC voltage source. Hence, η_{meas} includes the efficiencies of the DC–RF inverter, *K*-impedance inverter, coupled resonators, rectifier, and switching voltage regulator. The minimum input voltage V_{in}, which is defined in Fig. 18, with each vertical displacement was the value when V_{rec} reached 6.5 V. Figure 20(b) shows the simulated efficiency η_{sim}, which was defined as 2.5 W divided by the total output power from two square-wave voltage sources. The input voltage V_{in} was varied from 1 to 30 V at intervals of 1 V. The simulated efficiency was shown with the input voltage V_{in} that realized a power supply of 2.5 W. Both the simulation results and the measurement results showed that the efficiency curve as a function of the input voltage V_{in} with each vertical displacement has one peak and the peak efficiency is >50%, although the theoretical maximum efficiency without a suitable output filter does not reach 50%. Thus, the maximum efficiency point is successfully stabilized by the *K*-impedance inverter, and the transfer efficiency can be maximized by applying input voltage adjustment. Moreover, the fabricated WPT system could realize stable operation even when V_{rec} is equal to 6.5 V. Hence, the entire range of the input voltage to the switching regulator was stabilized. The proposed methods were thus validated by both measurements and simulations. There are voltage gaps of about 2 V between the input voltage values (V_{in}) to maximize the efficiency in the simulations and measurements, which are attributed to errors caused by modeling of the diodes, rectifier, RF power source, and switching voltage regulator in the simulations. The rectifier may cause errors owing to the parasitic resistance, capacitance, and inductance in the printed circuit board as well as individual differences in the Schottky barrier diodes employed in the rectifier. Two square-wave voltage sources were used to model the full-bridge class-D inverter; hence, the losses in the field effect transistors (FETs) and the effect of dead time were not considered in the simulations. The efficiency of the switching voltage regulator was assumed to be 90% in the simulations; however, the actual value varies between 88 and 93% depending on the input voltage to the regulator.

We also tried to transmit power without the *K*-impedance inverter, but it was impossible within the recommended current limitations of EPC9065 and the operation range of the input voltage of V7805-1000. This is because when R_{sr} is larger than $R_{sr(mpp)}$, the input impedance seen from the input of the transmitting resonator is less than $2r_1$ in a system without the *K*-impedance inverter, and a larger value of R_{sr} requires a larger output voltage V_{rec} to consume 2.5 W. Instead, we simulated the transfer efficiency without a *K*-impedance inverter. Figure 21(a) shows the simulated transfer efficiency as a function of the input voltage of the RF power source. The full-bridge rectifier was originally modeled with Schottky diodes (PMEG4020EPK); however,

Table 5. Measured value of $R_{eq} + jX_{eq}$ with vertical displacements.

0 cm	2 cm	4 cm	6 cm
$2.075 + j1.01\ \Omega$	$1.949 + j0.84\ \Omega$	$1.845 + j0.69\ \Omega$	$1.750 + j0.58\ \Omega$

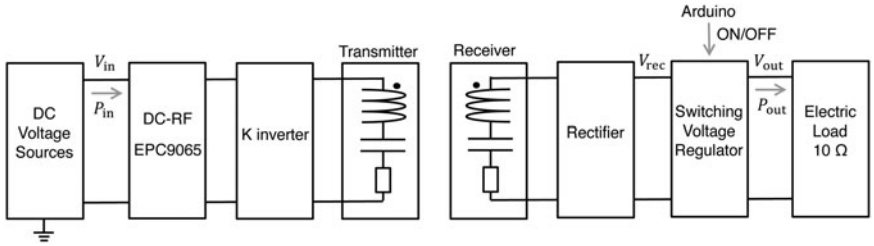

Fig. 18. Block diagram of experimental setup.

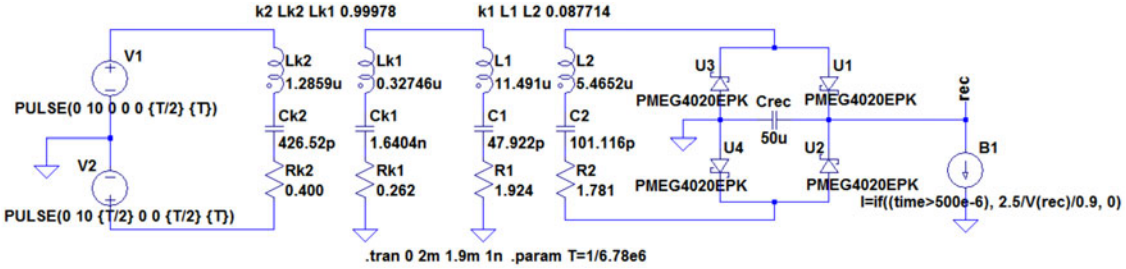

Fig. 19. Simulation setup for the verification of measurement results.

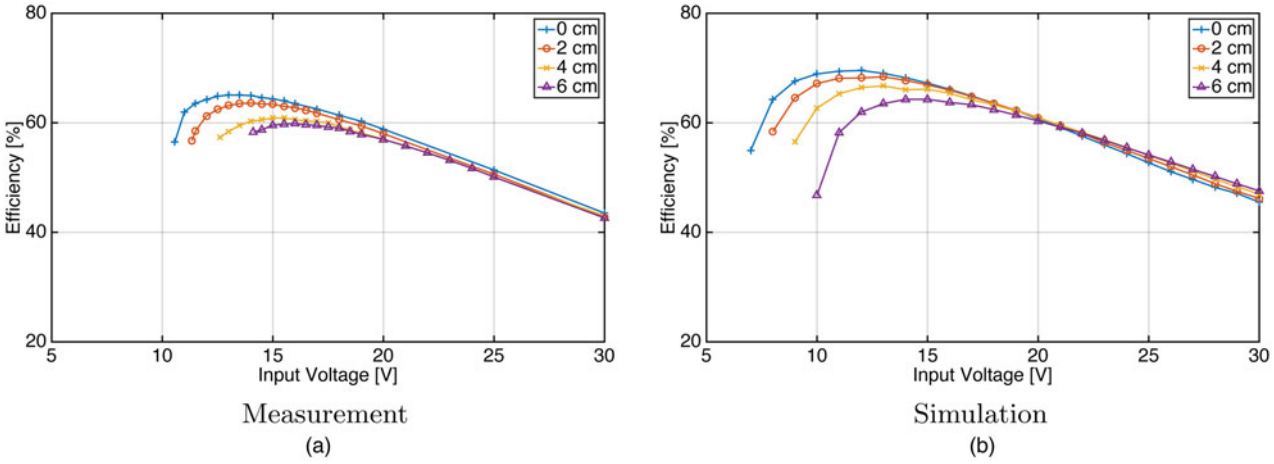

Fig. 20. Measured efficiency η_{meas} and simulated efficiency η_{sim} as a function of the input voltage V_{in} to a class-D inverter when the vertical displacement of the receiver is 0, 2, 4, and 6 cm.

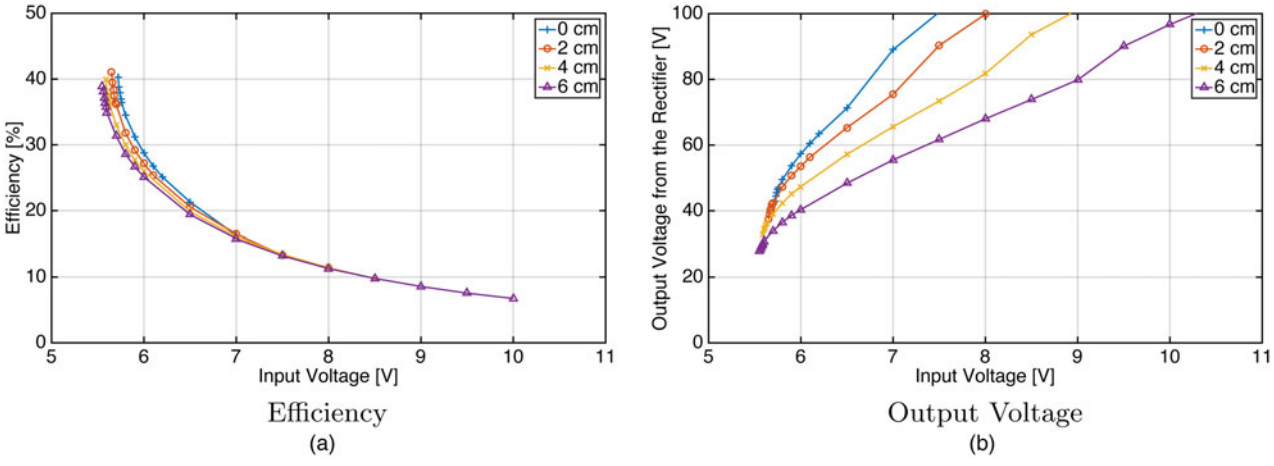

Fig. 21. Simulated efficiency η_{sim} and output voltage V_{rec} from the rectifier without the K-impedance inverter as a function of the input voltage V_{in} to a class-D inverter.

we used PMEG10020ELR in this simulation, because it was found that the output voltage V_{rec} exceeded 40 V in most of the simulation conditions, as shown in Fig. 21(b). The input voltage was varied at intervals of 0.01 V to find the minimum input voltage for realizing a power supply of 2.5 W. As the input voltage decreases to the minimum input voltage, the efficiency increases monotonically, but it does not reach 50%. This result supports the theoretical analysis and confirms the effectiveness of the *K*-impedance inverter.

VI. CONCLUSION

Instead of controlling the frequency or input voltage, using a switching regulator in the receiver side of a WPT system is one of the solutions to realize stable output voltage. However, this paper showed that the receiver-side switching voltage regulator drastically degrades the WPT efficiency because of its input resistance value at a stable operating point. Specifically, the input resistance value at a stable operating point is higher than the optimum resistance value in a WPT system with a class-D inverter and series-resonant transmitter and receiver. To maximize the transfer efficiency, we derived the input resistance value of the switching voltage regulator at a stable operating point, and we proposed a system design with a *K*-impedance inverter. The system with the receiver-side switching voltage regulator and the *K*-impedance inverter as an output filter in the RF power source achieved the optimum input voltage for maximizing the transfer efficiency. Simulations and measurements showed the effectiveness of the proposed methods. The proposed method is beneficial for wirelessly powering electric devices that require a constant operating voltage, such as home appliances, mobile phones, and micro-controller boards.

ACKNOWLEDGEMENTS

This work was supported by ERATO (Exploratory Research for Advanced Technology) of JST Strategic Basic Research Programs and a grant-in-aid for JSPS Fellows (26.7147).

REFERENCES

[1] Brown, W.C.: The history of power transmission by radio waves. IEEE Trans. Microw. Theory Tech., **32** (9) (1984), 1230–1242.

[2] Kurs, A.; Karalis, A.; Moffatt, R.; Joannopoulos, J.D.; Fisher, P.; Soljačić, M.: Wireless power transfer via strongly coupled magnetic resonances. Science, **317** (5843) (2007), 83–86.

[3] Karalis, A.; Joannopoulos, J.D.; Soljačić, M.: Efficient wireless non-radiative mid-range energy transfer. Ann. Phys., **323** (1) (2008), 34–48.

[4] Fisher, T.M.; Farley, K.B.; Gao, Y.; Bai, H.; Tse, Z.T.H.: Electric vehicle wireless charging technology: a state-of-the-art review of magnetic coupling systems. Wireless Power Transfer, **1** (2) (2014), 87–96.

[5] Kim, J.; Son, H.C.; Kim, D.H.; Park, Y.J.: Optimal design of a wireless power transfer system with multiple self-resonators for an LED TV. IEEE Trans. Consum. Electron., **58** (3) (2012), 775–780.

[6] Kang, S.H.; Nguyen, V.T.; Jung, C.W.: Analysis of WPT system using rearranged indirect-fed method for mobile applications, in 2015 IEEE Wireless Power Transfer Conf., Boulder, CO, USA, 2015, 1–4.

[7] RamRakhyani, A.K.; Mirabbasi, S.; Chiao, M.: Design and optimization of resonance-based efficient wireless power delivery systems for biomedical implants. IEEE Trans. Biomed. Circuits Syst., **5** (1) (2011), 48–63.

[8] Wei, W.; Kawahara, Y.; Kobayashi, N.; Asami, T.: Characteristic analysis of double spiral resonator for wireless power transmission. IEEE Trans. Antennas Propag., **62** (1) (2014), 411–419.

[9] Jonah, O.; Merwaday, A.; Georgakopoulos, S.V.; Tentzeris, M.M.: Spiral resonators for optimally efficient strongly coupled magnetic resonant systems. Wireless Power Transfer, **1** (1) (2014), 21–26.

[10] Awai, I.; Ishizaki, T.: Transferred power and efficiency of a coupled-resonator WPT system, in 2012 IEEE MTT-S IMWS IWPT, Kyoto, Japan, 2012, 105–108.

[11] Florian, C.; Mastri, F.; Paganelli, R.P.; Masotti, D.; Costanzo, A.: Theoretical and numerical design of a wireless power transmission link with GaN-based transmitter and adaptive receiver. IEEE Trans. Microw. Theory Techn., **62** (4) (2014), 931–946.

[12] de Rooij, M.A.: The ZVS voltage-mode class-D amplifier, an eGaN FET-enabled topology for highly resonant wireless energy transfer, in 2015 IEEE Applied Power Electron. Conf. and Expo, Charlotte, NC, U.S.A., 2015, 1608–1613.

[13] Lu, Y.; Ki, W.H.: A 13.56 MHz CMOS active rectifier with switched-offset and compensated biasing for biomedical wireless power transfer systems. IEEE Trans. Biomed. Circuits Syst., **8** (3) (2014), 334–344.

[14] Mizuno, K.; Miyakoshi, J.; Shinohara, N.: *In vitro* exposure system using magnetic resonant coupling wireless power transfer. Wireless Power Transfer, **1** (2) (2014), 97–107.

[15] Moriwaki, Y.; Imura, T.; Hori, Y.: Basic study on reduction of reflected power using DC/DC converters in wireless power transfer system via magnetic resonant coupling, in 2011 IEEE 33rd Int. Telecommunications Energy Conf., Amsterdam, Nederland, 2011, 1–5.

[16] Ishihara, H. et al.: A voltage ratio-based efficiency control method for 3 kW wireless power transmission, in 2014 IEEE Applied Power Electronics Conf. and Expo, Fort Worth, TX, USA, 2014, 1312–1316.

[17] Kim, N.Y.; Kim, K.Y.; Choi, J.Y.; Kim, C.W.: Adaptive frequency with power-level tracking system for efficient magnetic resonance wireless power transfer. IET Electron. Lett., **48** (8) (2012), 452–454.

[18] Gunji, D.; Imura, T.; Fujimoto, H.: Stability analysis of constant power load and load voltage control method for wireless in-wheel motor, in 2015 IEEE Int. Conf. on Power Electronics and ECCE Asia, Seoul, Korea, 2015, 1944–1949.

[19] Li, H.; Li, J.; Wang, K.; Chen, W.; Yang, X.: A maximum efficiency point tracking control scheme for wireless power transfer systems using magnetic resonant coupling. IEEE Trans. Power Electron., **30** (7) (2015), 3998–4008.

[20] Narusue, Y.; Kawahara, Y.; Asami, T.: Maximum efficiency point tracking by input control for a wireless power transfer system with a switching voltage regulator, in 2015 IEEE Wireless Power Transfer Conf., Boulder, CO, USA, 2015, 1–4.

[21] Ito, M. et al.: High efficient bridge rectifiers in 100 MHz and 2.4 GHz bands, in 2014 IEEE Wireless Power Transfer Conf., Jeju, Korea, 2014, 64–67.

[22] Dionigi, M.; Mongiardo, M.: CAD of efficient wireless power transmission systems, in 2011 IEEE Int. Microwave Symp. Digest, Baltimore, MD, USA, 2011, 1–4.

[23] Ean, K.K.; Chuan, B.T.; Imura, T.; Hori, Y.: Novel band-pass filter model for multi-receiver wireless power transfer via magnetic resonance coupling and power division, in 2012 IEEE Wireless and Microwave Technology Conf., Cocoa Beach, FL, USA, 2012, 1–6.

[24] Ishida, T.; Yamaguchi, K.; Ishizaki, T.; Awai, I.: Novel measurement technique of WPT circuits using VNA and its data transformation into 0-ohm system, in 2012 MTT-S IMWS IWPT, Kyoto, Japan, 2012, 231–234.

[25] Awai, I.: Basic characteristics of "Magnetic resonance" wireless power transfer system excited by a 0 ohm power source. IEICE Electron. Express, **10** (21) (2013), 20132008.

Yoshiaki Narusue received the B.E. and M.E. degrees in Information and Communication Engineering from the Graduate School of Information Science and Technology, The University of Tokyo, Tokyo, Japan, in 2012 and 2014, respectively. Currently, he is pursuing the Ph.D. degree in the same department. He received the second-best student paper award at the IEEE Radio and Wireless Symposium in 2013. His research interests mainly include wireless power transfer using magnetic resonant coupling and energy harvesting from microwaves. Mr. Narusue is a student member of the IEEE, IEICE, and IPSJ.

Yoshihiro Kawahara received the B.E., M.E., and Ph.D. degrees in Information and Communication Engineering from The University of Tokyo, Tokyo, Japan, in 2000, 2002, and 2005, respectively. Currently, he is an Associate Professor with the Department of Information and Communication Engineering, The University of Tokyo, Tokyo, Japan. He joined the faculty in 2005. From 2011 to 2013, he was a Visiting Scholar with the Georgia Institute of Technology, Atlanta, GA, USA. Further, he was a Visiting Assistant Professor with the Massachusetts Institute of Technology, Cambridge, MA, USA, in 2013. His research interests lie in the areas of computer networks and ubiquitous and mobile computing. He is currently interested in developing energetically autonomous information communication devices. Dr. Kawahara is a member of the IEICE and IPSJ. He also is a committee member of IEEE MTT TC-24 (RFID Technologies).

Tohru Asami received the B.E. and M.E. degrees in Electrical Engineering from Kyoto University, Kyoto, Japan, in 1974 and 1976, respectively, and the Ph.D. degree in information and communication engineering from The University of Tokyo, Tokyo, in 2005. In 1976, he joined KDD (KDDI), Tokyo, Japan. Since then, he has been working in several research areas such as UNIX-based data communication systems and network management systems. After serving as the CEO of KDDI R&D Laboratories, Inc., he joined the University of Tokyo in 2006 as a Professor with the Department of Information and Communication Engineering, Graduate School of Information Science and Technology. Professor Asami was a Vice Chairman on the Board of Directors of the Information and Systems Society at the Institute of Electronics, Information and Communication Engineers, Japan (IEICE-ISS), from 2003 to 2005.